Desalination 458 (2019) 54–65

Contents lists available at ScienceDirect

Desalination

journal homepage: www.elsevier.com/locate/desal

Design of spiral-wound electrodialysis modules

Natasha C. Wright*, Amos G. Winter V

Department of Mechanical Engineering, Massachusetts Institute of Technology, Cambridge, MA 02139, United States of America

ARTICLE INFO

Keywords:
Electrodialysis
Brackish groundwater
Spiral-wound
Desalination model

ABSTRACT

Spiral-wound electrodialysis (ED) modules are of interest because, in a parallel flow configuration where both the diluate and concentrate streams flow from the inner electrode to the outer electrode along a spiral path, the applied current density decreases as the concentration in the diluate stream and associated limiting current density (LCD) decrease. By matching the applied current density as closely as possible to the LCD at any given location in a stack, the required amount of membrane area is minimized, reducing capital cost. This work presents an analytical model for a spiral-wound ED module and experimental validation of that model using a prototype stack with two cell pairs and four revolutions. A constant voltage was applied and the total current and stream conductivities at mid-stack and the output were recorded. Experimental results agreed with the model for all parameters to within 15%. The model was used to explore the most cost-effective spiral stack designs for desalting brackish groundwater, examining both a standard Archimedean spiral (as is common for spiral-wound RO modules), and a novel ideal spiral. The ideal spiral shape was found to reduce total cost by 21% and capital cost by 39% with respect to an Archimedean spiral.

1. Introduction

Electrodialysis (ED) is a desalination technology that uses an electric current acting over a series of anion and cation exchange membranes (AEM and CEM, respectively) to drive salt transport. While improvements have been made to individual components, the basic architecture of ED stacks has not changed since the concept of a multi-compartment ED cell having alternating cation and anion exchange membranes was first proposed by Meyer and Strauss in 1940 [1]. Commercial ED stacks, manufactured for example by Suez Water Technologies & Solutions and Hangzhou Iontech, have a similar architecture in which flat, rectangular membranes and flow channels are sandwiched between two or more electrodes.

For any given ED stack having a set membrane area, the desalination rate is maximized when the applied current density (the amount of electric current per unit cross-sectional area of membrane) is maximized. However, this applied current density must lie below the limiting current density (LCD), the current density that results in a zero ion concentration at the membrane surface in the diluate channel. LCD is governed by diluate stream velocity, salt concentration, and channel spacer geometry. Studies that investigate the cost-optimal design of flat stack architectures reveal that if membrane costs are dominant over pumping costs (both capital and energetic), then operating close to the LCD at all points in the flow path within an ED stack is preferred [2,3].

Commercial ED systems typically run in continuous mode, where the flow path is designed to achieve the desired concentration reduction in a single pass through the system. In order to operate close to the LCD throughout the process, individual ED stacks are staged in series with decreasing applied voltage over each successive stage. As a result of this staging, the applied current density decreases as the diluate solution concentration and LCD also decrease. While it is possible to apply the voltages in the system such that the applied and limiting current densities match at the outlet of each stack in the series, the applied current density will be lower than the LCD at all other locations in the stacks due to the non-linear relationship between salt concentration and electrical resistance. Thus, conventional ED stacks operating under constant voltage cannot maintain matching applied current density and LCD at all locations along the flow path.

For the spiral-wound ED modules investigated in this work, the diluate and concentrate streams flow in parallel from an inner electrode to an outer electrode along a spiral path. Fig. 1 shows how the feed water enters the alternating CEMs and AEMs and separates into diluate and concentrate streams. This stack configuration is of interest because the applied current density decreases with each successive revolution of the spiral by nature of the increasing effective membrane area through which the current must pass. The applied current density thus decreases as the concentration in the diluate stream and associated LCD decreases. By matching the applied current density as closely as possible

* Corresponding author.
E-mail address: ncwright@mit.edu (N.C. Wright).

https://doi.org/10.1016/j.desal.2019.01.010
Received 24 September 2018; Received in revised form 30 December 2018; Accepted 10 January 2019

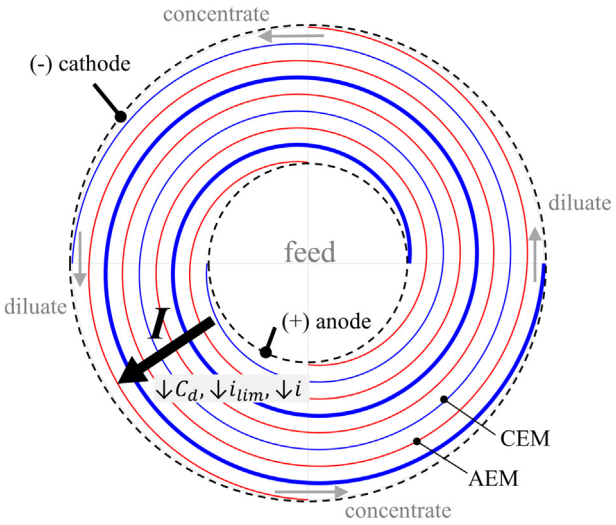

Fig. 1. A spiral-wound ED module in which feed water entering through a perforated center electrode flows between alternating anion (red) and cation (blue) exchange membranes, which have been wound in a spiral around the center electrode. A single membrane is shown in bold for visual clarity of the spiral shape. A voltage applied across the anode and cathode drives a current, I, which separates the feed into diluate and concentrate streams. Both the limiting and applied current densities (i_{lim} and i, respectively) decrease as the diluate concentration, C_d, decreases.

to the LCD at any given location in a stack, the required amount of membrane area is minimized.

Arden and Solt first patented the concept of a spiral-wound ED module in 1953 [4]. Solt went on to analytically model both parallel and cross-flow configurations with Wen and Sun in the early 1990s [5,6]. Wen et al. also tested a parallel flow spiral-wound ED stack experimentally [7], however, the performance was not compared to the analytical model in [5].

The work presented here expands on the previous literature by incorporating calculations of the limiting current density, electrical resistance in the fluid boundary layer, and the effects of spacer geometry into the analytical model. Incorporation of the LCD is critical, as the proposed benefit of a spiral stack is to maintain current density near limiting at all points along the spiral. This work also addresses the need for an experimentally validated analytical model for spiral ED modules, as well as a discussion on the effect that geometric and operating parameters have on performance. This parametric view of ED spiral stack behavior allows us to solve for both the capital and total cost-minimized spiral stack configurations. Finally, this work compares the cost-minimized configuration of a traditional Archimedean spiral to a novel spiral shape in which the radius varies along the length of the spiral to ensure that the applied current density and LCD not only decrease with each successive revolution, but match in value along the entire length of the spiral – a condition that is not possible to achieve with a standard Archimedean spiral.

2. Analytical model

The analytical model presented in this work is based on the model for standard flat stack configurations developed and experimentally validated in our previous work [8]. Only the modifications that are required to represent the spiral architecture are presented in this section.

The model describes a spiral design with a known inner electrode radius, r_0, number of cell pairs, N, and total number of revolutions, S, and calculates the desalination rate, membrane and electrode area, and energy consumption. In Section 4 we discuss the inverse problem of determining the optimal number of cell pairs, number of revolutions,

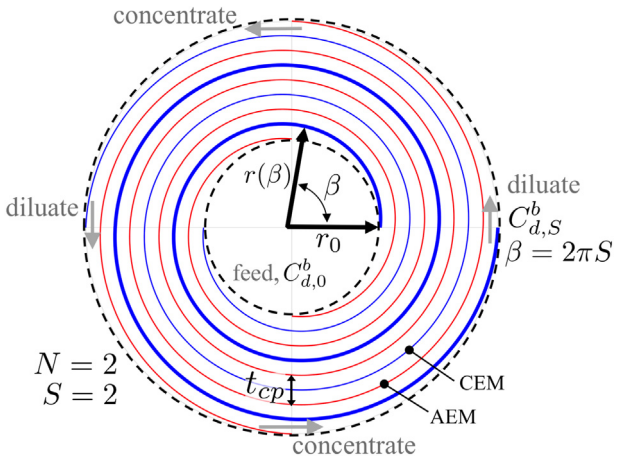

Fig. 2. The radius, r, of a standard Archimedean spiral increases at a constant rate equal to the cell pair thickness, t_{cp}, with each successive revolution. This Archimedean spiral stack has two cell pairs, N, and two total revolutions, S, ending at a final angle of $\beta = 2\pi S$. The bulk concentration of the diluate at the end of any given revolution, s, is denoted as $C^b_{d,s}$.

inner electrode radius, and applied voltage such that matching between LCD and applied current density occurs at the beginning and end of the spiral (using an Archimedean spiral shape), and then along the length of the entire spiral (using a novel ideal spiral shape).

2.1. Defining the Archimedean spiral

An Archimedean spiral (also called an arithmetic spiral) is a spiral in which the radius increases by a constant value with each successive revolution. The Archimedean spiral thus defines the shape that would be achieved if standard ED cell pairs were wrapped around a center electrode, since the thickness of the cell pairs remains constant. This shape is also that employed by spiral-wound RO modules. The local radius of an ED stack wrapped as an Archimedean spiral is defined in polar coordinates as

$$r(\beta) = r_0 + \frac{Nt_{cp}}{2\pi}\beta, \tag{1}$$

where r_0 is the radius of the center electrode, β is the angle around the spiral, and t_{cp} is the thickness of a single cell pair, given as the sum of channel heights, h, and the AEM/CEM membranes thicknesses (l_a and l_c, respectively) such that $t_{cp} = 2h + l_a + l_c$. Fig. 2 shows a two cell pair ($N = 2$), two revolution ($S = 2$) Archimedean spiral.

2.2. Total membrane area

The length of a single membrane is found using the equation for the arc length of a curve in polar coordinates

$$L = \int_0^{\beta_f} \sqrt{r(\beta) + \frac{dr}{d\beta}} \quad d\beta, \tag{2}$$

where the integral is evaluated from 0 to $\beta_f = 2\pi S$, the angle at the end of the spiral. The total volumetric flow rate of the diluate Q_d (m^3/s) is

$$Q_d = NWhu_{ch}\epsilon, \tag{3}$$

where W is the width of a single membrane (m), h is the channel height (m), u_{ch} is the spacer-filled channel velocity (m/s), and ϵ is the void fraction. The total membrane area in the spiral is then given by

$$A_{\text{total}} = 2NLW, \tag{4}$$

while the projected area for any given membrane segment j covering less than 2π radians can be approximated by

$$A_j = (\beta_2 - \beta_1)r(\beta_1)W, \tag{5}$$

where r is evaluated at β_1. As $(\beta_2 - \beta_1)$ goes to zero, the stack is segmented into smaller paths for the current to flow and the discrete analysis approaches the continuous solution.

2.3. Mass transfer

We begin by neglecting the contribution of back-diffusion due to the ionic concentration gradient between the concentrate and diluate channels. Doing so allows us to solve the set of equations in this section without the use of an iterative solver. The effect that this assumption has on predicted salt removal rates is discussed in Section 3.3. The quantity of salt removed in a single pass through the spiral is then a result of migration due to the applied current I alone and is calculated by

$$(C^b_{d,0} - C^b_{d,S}) = \frac{I\phi SN}{zFQ_d}, \tag{6}$$

where $C^b_{d,0}$ is the feed water salinity in the bulk solution (mol/m^3) at the center electrode, $C^b_{d,S}$ is the final diluate salinity in the bulk solution (mol/m^3) as it leaves the stack at the final revolution S, ϕ is the current leakage factor, z is the ion charge number, and F is Faraday's constant (C/mol).

Because the same amount of current must pass through each successive revolution of the spiral, the change in concentration must also be the same ($C^b_{d,0} - C^b_{d,1} = C^b_{d,1} - C^b_{d,2}$). Eq. (6) thus leads to the equation for the diluate concentration in any given revolution of the spiral,

$$C^b_{d,s} = C^b_{d,0} - \frac{I\phi sN}{zFQ_d}, \tag{7}$$

where s is the revolution number, counting outwards from the inner electrode.

2.4. Limiting current

The maximum current I_{lim} that can be applied to the spiral is calculated from the limiting current density i_{lim} with

$$i_{lim} = \frac{I_{lim}}{\phi_A A} = \frac{C^b_d zFk}{t^{mem} - t_{+,-}} = \frac{C^b_d zFD_{aq}0.29Re_d^{0.5}Sc^{0.33}}{d_h(t^{mem} - t_{+,-})}, \tag{8}$$

where definitions of the area porosity, ϕ_A, Reynold's number, Re, Schmidt number, Sc, mass transfer coefficient, k, hydraulic diameter, d_h, diffusion coefficient of the aqueous solution, D_{aq}, and the transport numbers, t^{mem} and $t_{+,-}$ are as defined in [8]. Values for the transport properties used throughout this work are listed in Table 1.

Introducing a desired current ratio ($\gamma = I/I_{lim}$) and setting the applied current I in Eq. (6) equal to the adjusted limiting current γI_{lim}, we can solve for the inner electrode radius that would facilitate the desired current to be applied at the beginning of the flow path when $C^b_d = C^b_{d,0}$ as

$$r_0 = \frac{(1 - CR^{-1})u_{ch}^{1/2}}{S}\xi,$$

where

$$\xi = \frac{h^{3/2}\varepsilon^{3/2}\mu^{1/6}(t^{mem} - t_{+,-})}{0.29\pi\phi\gamma(2 + 8(1-\varepsilon))^{1/2}\rho^{1/6}D_{aq}^{2/3}\phi_A}, \tag{9}$$

and where $CR = C^b_{d,0}/C^b_{d,S}$, the ratio of feed to product water concentration. Note that if a certain membrane and spacer type is assumed (properties of which are used to calculate ξ), the full spiral shape (Eq. (1)) can be defined using only CR, the channel velocity, u_{ch}, the number of revolutions, S, and the number of cell pairs, N.

Table 1
Global modeling parameters. Discussion on the sensitivity of transport properties to concentration and temperature can be found in [8].

Parameter	Value	Ref
D^{AEM} (m^2/s)	3.28×10^{-11}	[9]
D^{CEM} (m^2/s)	3.28×10^{-11}	[9]
D_{aq} (m^2/s)	1.6×10^{-9}	[10]
t_+	0.39	[11]
t_-	0.61	[11]
t^{mem}	1	[12]
ϕ	1	

2.5. Voltage potential

Just as with standard flat-stack ED architectures, the spiral ED stack is modeled as an analogous DC circuit. However, the spiral is distinct in that the current passes through the same solution S times and the area of each successive flow channel/membrane increases as you move from the inner to outer electrode. The voltage at the electrodes, E_{total}, is related to the current by,

$$E_{\text{total}} = E_{\text{el}} + \frac{I}{\phi_A}\sum_{j=1}^{J}\left(\frac{R^b_{d,j} + R^{BL}_{d,j} + R^{\text{mem}}}{A_{d,j}} + \frac{R^b_{c,j} + R^{BL}_{c,j} + R^{\text{mem}}}{A_{c,j}}\right) + \sum_{j=1}^{J} E_{\text{mem},j}. \tag{10}$$

Here j indicates the channel location such that $j = 1$ is the diluate and concentrate channel closest to the inner electrode, and that a total of $J = NS$ diluate channels and $J = NS$ concentrate channels exist between the inner and outer electrode. The area resistances $R^b_{d,j}$, $R^{BL}_{d,j}$, $R^b_{c,j}$, and $R^{BL}_{c,j}$ are associated with the bulk and boundary layer fluid in the diluate and concentrate streams, respectively ($\Omega\,m^2$). The average area resistance of the AEM and CEM exchange membrane is given by R^{mem} ($\Omega\,m^2$). $A_{d,j}$ and $A_{c,j}$ are the projected areas of the diluate and concentrate channel (m^2) such that both increase as j increases, in accordance with Eq. (5). E_{mem} is the potential across each membrane pair; it is a function of the concentration at the membrane wall and thus also changes based on channel location, j. Finally, E_{el} is electrode potential difference. Given a known bulk concentration and effective area for each channel location, each of the terms in Eq. (10) can be calculated as presented in [8].

2.6. Specific energy

The total specific energy Γ_{total} (J/m^3) is given by the sum of the energy required for desalination and for pumping as,

$$\Gamma_{\text{total}} = \frac{IE_{\text{total}}}{Q_d} + \frac{2P}{\eta_{\text{pump}}}, \tag{11}$$

where P is the pressure drop over the stack (Pa) and η_{pump} is the efficiency of the pump. It is assumed that the volumetric flow rate and pressure drop is the same in the concentrate and diluate streams. The pressure drop in the spiral is modeled using the correlation developed by Ponzio et al. [13], which was found to be the best match to an existing commercial ED system in [8].

2.7. Defining the ideal spiral

Plotting γi_{lim} and i as a function of the local concentration in the spiral (Fig. 3) reveals that although an Archimedean spiral could allow for matching applied and adjusted limiting current densities at the inlet and outlet of the stack, there remains a significant amount of wasted membrane capacity in the middle revolutions. The Archimedean spiral shape provides for a linearly decreasing diluate concentration with each successive revolution (Eq. (7)), resulting in a linearly decreasing LCD

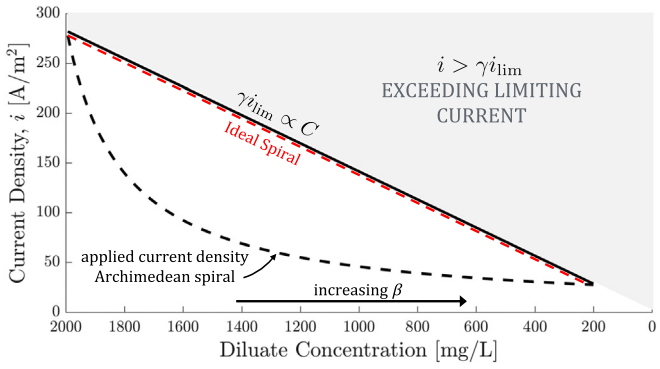

Fig. 3. In an Archimedean spiral, the stack can be designed such that the applied (black dashed line) and adjusted limiting (solid line) current densities match at the beginning and end of the stack. However, it is not possible to design an Archimedean spiral with a match at all locations. A new ideal spiral shape is required to allow for continuous matching (red dashed line).

($i_{lim} \propto C_d^b$, Eq. (8)). However, the radius, and thus the effective area, increases linearly with each revolution of the spiral. As a result the applied current density (which scales as I/A) will not decrease linearly as desired, rather it will decrease inversely with each successive revolution.

Combining Eqs. (7)–(9) and setting I (Eq. (7)) equal to γI_{lim} (Eq. (8)) for all C_d, we can solve for the equation of a spiral that would allow the local applied and adjusted limiting current densities to match along the entire length of the spiral. This spiral is described in polar coordinates as

$$r(\beta) = \frac{r_0}{1 - \beta\left(\frac{1 - CR^{-1}}{\beta_f}\right)}, \tag{12}$$

where CR is the desired concentration ratio $C_{d,0}^b / C_{d,S}^b$.

3. Experimental validation of the Archimedean spiral model

A prototype spiral wound ED stack was assembled and instrumented to validate the analytical model presented in Section 2. The experimental setup and results are described here.

3.1. Prototype stack design

A photo of the prototype stack at three stages in the assembly process is shown in Fig. 4, a schematic of the stack is shown in Fig. 5, and Table 2 lists the prototype stack parameters required for comparison with the analytical model. The inner electrode was made from a grade 2 titanium tube with 50.8 mm outer diameter and 0.89 mm wall thickness; 6.35 mm diameter holes were added to allow water to enter the flow channels. Two cell pairs (20.5 cm membrane width, 91.4 cm individual membrane length) allowed four full revolutions before reaching the outer electrode, which was made from 0.13 mm thick 316SS (stainless steel) foil. Suez Water Technologies & Solutions AR204SZRA anion exchange membranes and CR67HMR cation exchange membranes, both homogeneous, were used. Membrane resistances were taken from the manufacturer data sheet, where the reported value was measured in 0.01N NaCl solution. The mesh spacer was made from Conwed Plastics' 31 mil RO spacer material.

Clear PVC pipe (inner diameter 15.8 mm) cut in half lengthwise was used to collect water as it exited the stack. 316SS tubing was inserted

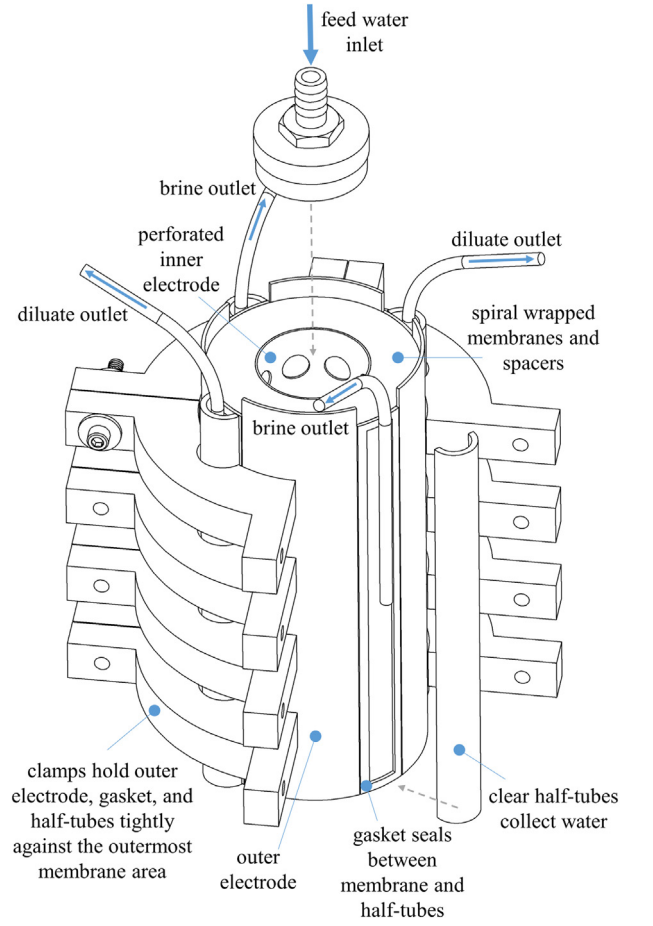

Fig. 5. Simplified CAD representation of the prototype spiral stack. Final resin seal not shown.

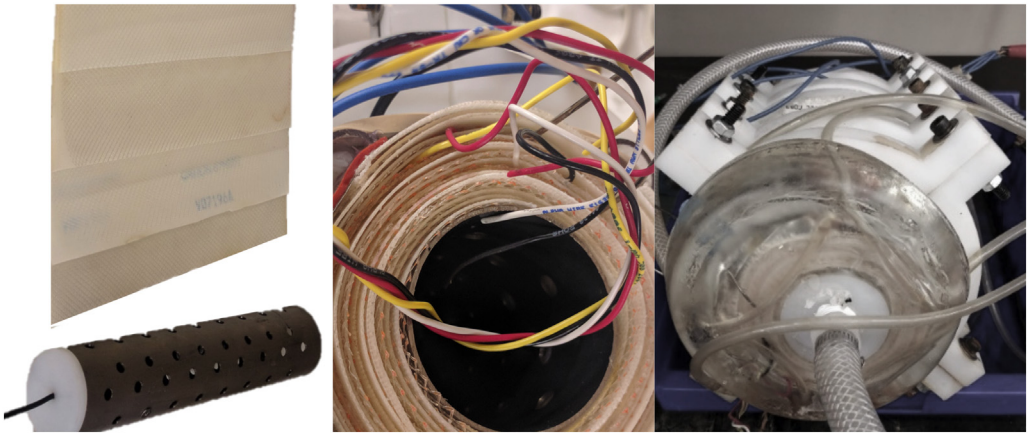

Fig. 4. The prototype used for model validation was constructed by rolling two membrane/spacer cell pairs around a titanium inner electrode (left) to produce a spiral shape (center). The spiral was sealed by compressing the outer electrodes against the membrane surface using clamps made out of HDPE and using epoxy resin to seal and cap the ends (right).

Table 2
Stack parameters.

Membrane properties	
Supplier	Suez
AEM model	AR204SZRA
CEM model	CR67HMR
AEM resistance (Ω cm^2)	7
CEM resistance (Ω cm^2)	10
AEM thickness (mm)	0.5
CEM thickness (mm)	0.6
Spacer properties	
Supplier	Conwed Plastics
Model	X0B354
Filament pitch (mm)	2.9 ± 0.1
Filament diameter (mm)	0.53 ± 0.03
Spacer thickness (mm)	0.76 ± 0.01
Spacer area porosity	0.67 ± 0.02
Spiral properties	
Flow path width (cm)	17.5
Flow path length (cm)	91.4
Number of cell pairs	2
Number of revolutions	4
Inner electrode radius (cm)	2.54
Channel height (mm)	0.82 ± 0.02
Calculated void fraction	0.83 ± 0.03
Electrode coverage	0.79 ± 0.03
Adjusted area porosity	0.53 ± 0.08

into the spiral one-third and two-thirds of the way along the membrane length and used to collect mid-stack water conductivity. Clamps were designed out of HDPE sheet to compress the half-tubes and their gaskets to the membranes. Finally, West System 105 and 207 epoxy resin and hardener was used to seal the ends of the stack. The epoxy serves as a replacement for the gasket material that lines the perimeter of traditional flat-stack spacer designs, and ensures that the solution flows from the inner electrode to the outer, without coming out the ends of the spiral. Prior testing showed that the epoxy rose 1.5 cm into the flow channels. As a result, the effective membrane width decreased to 17.5 cm; W is set equal to this value in the model comparisons.

3.2. Experimental setup

The diluate and concentrate streams were run in continuous mode, flowing in a parallel configuration from the inner electrode tube to the outer collection tubes. The feed solution was prepared using deionized water and the appropriate amount of reagent grade NaCl. A Shurflo 4008-101-E65 pump was used to provide feed solution to the stack; flow rate was controlled manually using a butterfly valve and measured using a Blue-White Industries F-1000-RB paddle wheel flowmeter (± 0.2 L/min). It is assumed that the flow divides equally between the concentrate and diluate channels providing 50% recovery. A Dr. Meter HY3005F-3 power supply was used to apply a constant voltage (± 0.1 V) across the electrodes and measure current (± 0.01 A). The mid-stack and final water stream conductivities were recorded manually over a period of 10 min for each test. Conductivity (± 1% of reading) and temperature (± 0.1 °C) measurements were taken using a Myron 4PII meter. Experimental error bars in the following tables and figures are reported as the quadrature of the sensor accuracy (given in this paragraph) and the 95% confidence interval over 5 measurements taken over the course of each experiment.

3.3. Results and discussion

Table 2 lists the prototype stack parameters required for comparison with the analytical model. Note that while a spacer thickness of 0.76 mm was measured prior to rolling the spacer, we were not able to roll the spiral tightly enough to ensure that the channel height was equal to the spacer thickness at all points in the stack. This was confirmed when measurements taken of the outside diameter of the spiral revealed its diameter to be 94.8 mm, whereas the calculated diameter with a spacer thickness of 0.76 mm should be 92.7 mm. Instead, we back-calculated the average channel height (h = 0.82 mm), and correspondingly updated the void fraction calculation from that found in [8] to Eq. (13), where d_f is the filament diameter (mm) and l_f is the filament pitch (mm). This resulted in an estimated void fraction of $\epsilon = 0.83$.

$$\epsilon = 1 - \frac{\pi d_f^2 (2l_f - d_f)}{4hl_f^2} \tag{13}$$

Additionally, the fractional membrane area available for ion transport, which is typically set to the area porosity of the mesh spacer in the flow channels (ϕ_A = 0.67), needs to be adjusted. The outer electrode sheets covered only 79% of the outermost membrane area in order to leave space for the water collection half-tubes. It is assumed that this coverage affects the area available for ion transport in the same way as the spacer area porosity. An adjusted area porosity representing the combined affects of the spacer porosity and electrode coverage is applied, such that ϕ_A = (0.79)(0.67) = 0.53. Note that there is also a porosity (0.90) associated with the inner electrode due to the holes added for feed water passage. While this porosity was not included in the calculation of the adjusted area porosity, its potential effect is included in the calculation of the uncertainty (± 0.08).

Table 3 presents the time averaged results from the experiment alongside the model prediction of the same parameters for all five tests. Note that the experimentally measured applied current, feed water conductivity, and flow rate served as inputs to the model; voltage potential, specific energy, and product, brine, and mid-stack conductivities were model outputs. Measurements matched the model within 1–15% (average 7%) for the voltage potential and specific energy, and within 1–11% (average 5%) for the conductivities.

Table 3
Experimental measurements and modeled results for five tests on the prototype Archimedean spiral ED stack, each of which had different feed water concentration and applied voltages. Measurements matched model values within 1–15% (average 7%) for voltage potential and within 1–11% (average 5%) for the conductivities. As direct measurement was not possible, channel velocity u_{ch} and specific energy for desalination Γ_{desal} were calculated using Eqs. (3) and (11), respectively.

Parameter	Test 1		Test 2		Test 3		Test 4		Test 5	
	Exp	Model	Exp	Model	Exp	Model	Exp	Model	Exp	Model
Voltage [V]	7.5 ± 0.1	7.6	8.0 ± 0.1	8.0	10.0 ± 0.1	11.0	14.0 ± 0.1	12.8	10.0 ± 0.1	8.5
Current [A]	0.95 ± 0.30	0.95	1.44 ± 0.02	1.44	2.53 ± 0.03	2.53	2.30 ± 0.05	2.30	2.94 ± 0.06	2.94
Flow rate [L/min]	2.07 ± 0.22	2.07	2.03 ± 0.20	2.03	1.98 ± 0.20	1.98	2.46 ± 0.22	2.46	2.65 ± 0.36	2.65
Channel velocity [cm/s]	7.2 ± 0.9	7.2	7.1 ± 0.8	7.1	6.9 ± 0.8	6.9	8.6 ± 0.9	8.6	9.3 ± 1.4	9.3
Feed conductivity [μS/cm]	1436 ± 16	1436	2149 ± 23	2149	3022 ± 31	3022	1983 ± 42	1983	4503 ± 46	4503
Product conductivity [μS/cm]	971 ± 11	943	1495 ± 24	1402	1903 ± 22	1697	940 ± 45	988	3471 ± 112	3389
Brine conductivity [μS/cm]	1882 ± 21	1921	2882 ± 35	2883	4231 ± 50	4312	2881 ± 67	2950	5380 ± 78	5597
Mid-stack diluate 1 conductivity [μS/cm]	1240 ± 14	1191	1880 ± 29	1778	2567 ± 28	2365	1524 ± 34	1490	4077 ± 42	3948
Mid-stack diluate 2 conductivity [μS/cm]	1079 ± 12	1067	1638 ± 40	1591	2191 ± 38	2033	1246 ± 33	1240	3774 ± 44	3669
Specific energy [kWh/m^3]	0.06 ± 0.02	0.06	0.09 ± 0.01	0.09	0.21 ± 0.02	0.23	0.22 ± 0.02	0.20	0.18 ± 0.03	0.16

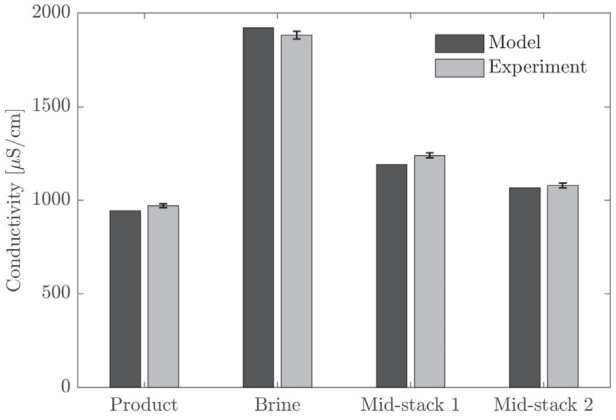

Fig. 6. Conductivity measurements for Test 1 shown in relationship to the model prediction.

The conductivity results for Test 1 are shown as a bar graph in Fig. 6 in order to better visualize the trend in the data. We note, for example, that the model slightly under predicts the experimental values in the diluate stream, while over predicting the experimental values in the brine stream. This trend was present for all tests except Test 4. This difference is expected given the decision to neglect back diffusion in the model, allowing the set the equations presented in Section 2 to be solved directly without iteration.

There are a number of design changes that could be incorporated in the next prototype stack to help determine the source of any additional error between model and experiments, as well as improve its overall performance and life. First, the small tubes inserted in two locations in the stack to probe for concentration should be added to every revolution, and in both the diluate and concentrate streams, allowing for better accounting of propagated error. Currently, the first membrane layer does not lay perfectly flat on the inner electrode, resulting in a fluid layer between the two surfaces and increased electrical resistance. A better method of assembling the spiral that would allow for a flush fit along the center electrode is needed. The stainless steel outer electrode and titanium inner electrode should be replaced with coated titanium to avoid development of pitting and rust. While these improvements are in progress, the present stack proved sufficient for initial validation of the analytical model and for recording the overall feasibility of desalinating using a spiral-wound ED module.

4. Cost-minimized spiral designs

With confidence that the spiral ED stack model adequately predicts behavior, we next aimed to identify the Archimedean and ideal spiral geometries and operating parameters that could provide the lowest 10-year total cost and capital cost. We first consider desalination of 2000 mg/L NaCl feed water to product water of 200 mg/L at a rate of 1000 L/h, with sensitivity to both concentrations explored in Section 5. This case study, as well as the cost basis described in the following section, were selected due to their applicability for village-scale desalination in remote areas of India [14]. Note that the fractional membrane area available for ion transport ϕ_A and void fraction ϵ were set to 0.56 and 0.80, respectively, throughout the cost-minimization trials.

4.1. Calculation of capital and total cost

The calculation of capital cost includes the cost of the diluate and concentrate pumps and the stack cost (assuming \$1200/m^2 electrode area, \$40/m^2 membrane area, \$10/m^2 spacer area). The total 10-year cost assumes 10,000 L/day total production and includes the capital cost, 10% interest over 5 years, \$0.10/kWh for both pumping and desalination energy, and pump replacement in the fifth year. A full description and justification of the these calculations as well as the pump cost and efficiency model are included in Appendix A.

4.2. Bounds and constraints

For all Archimedean spiral designs, we ensure that the applied current density is equal to the adjusted LCD ($\gamma = 0.7$) at the beginning and end of the spiral, where γ was set based on the recommendation provided by the American Water Works Association for commercial ED systems [15]. For ideal spiral designs, the applied current density is equal to the adjusted LCD ($\gamma = 0.7$) at all points along the spiral. In both cases, the spiral must complete a minimum of one full revolution ($\beta_f \geq 2\pi$). The design variables and associated bounds investigated for both cases are the channel height (0.3 mm $< h <$ 1.0 mm), the spacer-filled channel velocity (6 cm/s $< u_{ch} <$ 20 cm/s), and number of cell pairs ($1 < N < 300$).

There are two constraints on the number of cell pairs that a single spiral can hold. Both the Archimedean and ideal spiral shapes are constrained by the number of cell pairs that can start from the inner electrode,

$$2\pi r_0 \geq N t_{cp}. \tag{14}$$

The ideal spiral is additionally constrained by the number of cell pairs that can fit in the difference between the radius at $\beta = 0$ and $\beta = 2\pi$,

$$r(\beta = 2\pi) \geq N t_{cp} + r_0. \tag{15}$$

Detailed steps for calculating the capital and 10-year total cost using the equations in Section 2 and Appendix A along with these constraints can be found in Appendix B.

4.3. Cost-minimization results

An initial exploration of the design space using a full-factorial design of experiments (DOE) revealed that all points on the Pareto front utilize the smallest channel thickness (0.3 mm), which is consistent with previous literature on the optimization of ED stacks for brackish water desalination [3,16]. Pareto front designs also utilize the maximum number of cell pairs (Eqs. (14) and (15)) which acts to minimize the membrane and electrode width, W, for any given production rate. As a result, a full optimization algorithm is not required, and the Pareto fronts (Fig. 7) are solved for directly by varying u_{ch} alone. Specifically, increasing u_{ch} increases the LCD, which increases the applied current density, decreasing the total membrane area required and the resulting capital cost. However increasing u_{ch} also increases the specific energy consumption for both pumping and desalination, causing an increase in

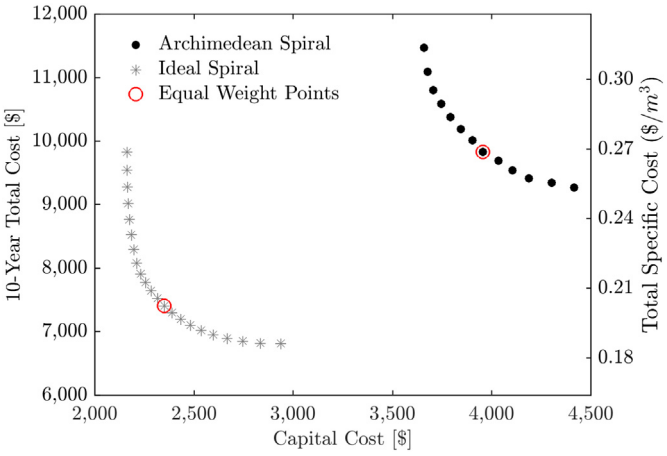

Fig. 7. A comparison of the capital cost vs. total cost Pareto fronts governing the Archimedean spiral and ideal spirals. The red open circles denote the designs that place equal importance (weight) on the total and capital cost.

Table 4
Pareto front geometries and operation conditions for the Archimedean spiral.

Parameter	Lowest capital cost	Lowest total cost	Equal weight
S [–]	1.4	1.4	1.4
N [–]	222	156	187
h [mm]	0.3	0.3	0.3
W [cm]	3.7	10.5	6.2
r_0 [cm]	6.0	4.3	5.1
r_S [cm]	59.1	41.6	49.8
A_{total} [m^2]	48.3	68.4	57.2
u_{ch} [cm/s]	14	7	10
$i_{j=1}$ [A/m^2]	330	232	278
P [kPa]	682.6	227.8	389.0
Γ_{desal} [kWh/m^3]	0.36	0.29	0.32
Γ_{pump} [kWh/m^3]	1.27	0.42	0.72
Stack cost [$]	2599	3782	3115
Capital cost [$]	3485	4350	3795
Total cost [$]	11,417	8898	9497

Table 5
Pareto front geometries and operation conditions for the ideal spiral.

Parameter	Lowest capital cost	Lowest total cost	Equal weight
S [–]	1.0	1.0	1.0
N [–]	335	205	277
h [mm]	0.3	0.3	0.3
W [cm]	2.1	9.4	3.8
r_0 [cm]	9.1	5.6	7.5
r_S [cm]	90.7	55.5	75.2
A_{total} [m^2]	24.9	40.6	30.0
u_{ch} [cm/s]	16	6	11
$i_{j=1}$ [A/m^2]	357	219	296
P [kPa]	498.7	99.4	246.7
Γ_{desal} [kWh/m^3]	0.70	0.49	0.61
Γ_{pump} [kWh/m^3]	0.93	0.18	0.46
Stack cost [$]	1405	2461	1735
Capital cost [$]	2162	2939	2316
Total cost [$]	9551	6818	7527

the total 10-year cost. The parameters that govern the lowest capital cost and lowest 10-year total cost designs are shown in Tables 4 and 5, along with the parameters for the result that places equal importance (weight) on both cost objectives.

5. Discussion

The ideal spiral is able to achieve 21% lower total cost and 39% lower capital cost than the Archimedean spiral for the design where both costs are equally weighted, denoted by the red equal weight points in Fig. 7. The shape of the spiral for both the Archimedean and ideal designs at these points are shown in Fig. 8. While the Archimedean spiral requires 1.4 revolutions to achieve the desired concentration change, the ideal spiral shape requires 1.0 revolutions, resulting in less total membrane area (30.0 vs 57.2 m^2), lower pressure drop (246.7 vs 389.0 kPa), and a resulting lower capital cost. Note that for the ideal spiral the outer electrode radius is quite large for this CR, at 79 cm, and the membrane width small at only 3.8 cm. The stacks would resemble discs, rather than long tubes (Fig. 8, top). The width of the membrane, however, is set by the desired volumetric flow rate (Eq. (3)), thus higher production capacity would be achieved by increasing the width of the membrane (thickness of the disc) while maintaining the value of all other parameters.

5.1. Design sensitivity to concentration ratio

To understand the sensitivity of the ideal spiral stack designs to changing feed and product water concentrations, Pareto fronts for five scenarios are shown in Fig. 9. Focusing first on the star markers, we see that the capital cost is nearly independent of the feed water concentration, so long as the concentration ratio is the same (here $CR = 10$). Higher feed water concentration requires more energy for desalination however, and thus the total 10-year cost increases as expected.

Maintaining the feed water concentration while increasing the product water concentration from 200 mg/L to 300 mg/L reduces both the capital and total costs by more than 20% at equivalent points on the Pareto front. Thus if reducing cost is an objective, it is important to consider choosing a product water concentration that is as high as acceptable.

5.2. Potential for staging of spiral stacks

A single stack with $CR = 8$ would have the same concentration reduction as three stacks in series, each with $CR = 2$. Fig. 10 shows the relationship between the spiral angle β and the local spiral radius $r(\beta)$ for various ideal spirals having different numbers of total revolutions, S, and concentration ratios, CR. Table 6 shows key stack parameters for the different values of CR and S given in Fig. 10. We observe that:

1. As S increases or CR decreases, the inner electrode radius decreases, resulting in a decrease in the number of cell pairs (Eqs. (14) and (15)).
2. For any given CR, the electrode area increases more rapidly than the membrane area decreases, as the number of revolutions increases from $S = 1$ to $S = 3$. Additionally, the electrode area ($1200/$m^2$) is more costly than membrane area ($100/$m^2$ cell pair). Both factors lead to a stack capital cost that is significantly more expensive for spirals having more revolutions.
3. For any given CR, the pressure drop over the stack, and thus specific energy required for pumping Γ_{pump}, is approximately the same regardless of the number of revolutions in the stack. Additionally, three $CR = 2$ stacks in series, having a net effect of $CR = 8$, have a total pressure drop approximately equal to that of a single $CR = 8$ stack. This result is due to both the 3-stage and single-stage configurations having the same total flow path length, the only factor affecting pressure drop in the presented cases since spacer geometry and linear flow velocities are the same.
4. The electrode radii for the cases shown range from 1.0 cm to 43.2 cm. Both extremes may be difficult to manufacture and thus further investigation into a feasible range is required.

As lower CR stacks have smaller inner and outer electrode radii (Fig. 10) and fewer cell pairs (Table 6), both of which could make the stack easier to manufacture; it is prudent to consider the effect of staging multiple smaller CR stacks in series. Cost-minimization was completed for a three-stage ideal spiral system in which each stack has $CR = 2.15$, for a total of $CR = 10$, to match the single stage Archimedean and ideal spiral scenario investigated in Section 4. When total and capital cost are equally weighted, the three stacks each have an inner radius of 5 cm, outer radius of 10.8 cm, membrane width of 24.2 cm, 34 cell pairs, and operate at 14 cm/s (Fig. 11). A component cost comparison between this system and the previous design for a single stage ideal spiral is shown in Fig. 12. The total and capital cost of the system increases over the single stage system. In order to select the lowest cost system staging, more information is needed on the cost and feasibility of manufacturing cylindrical electrodes of various sizes.

5.3. Merits of a cross-flow configuration

In this work we have thus far discussed a parallel flow configuration where the feed water divides equally into diluate and concentrate from the center electrode. This configuration becomes difficult to implement as the number of cell pairs (and thus collection tubes at the outer electrode) increases. Additionally, achieving a recovery greater than

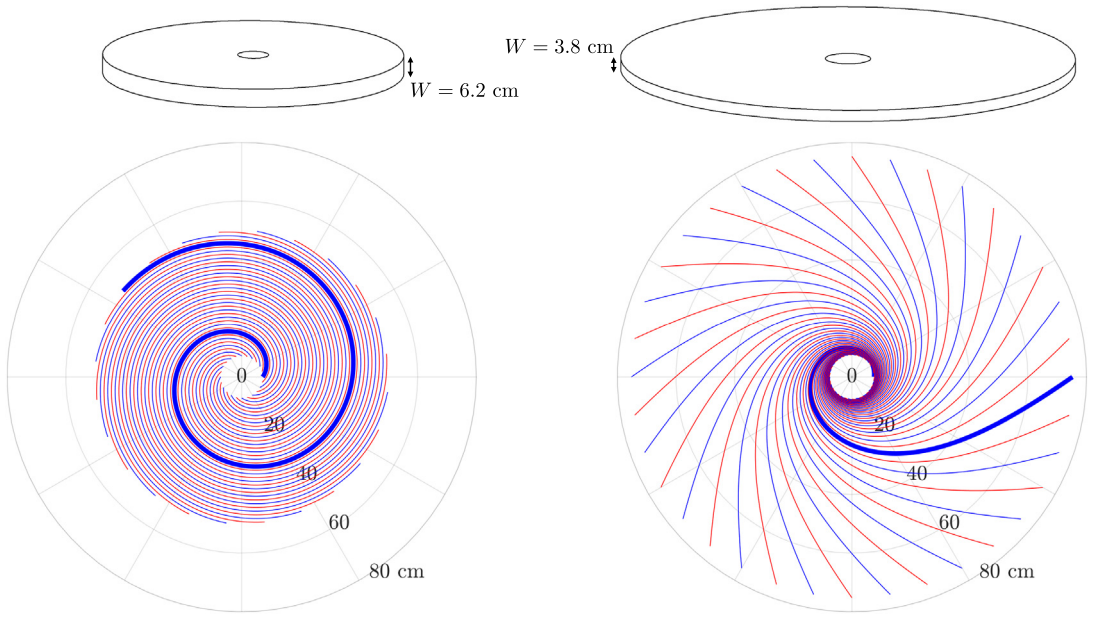

(a) Achimedean Spiral (b) Ideal Spiral

Fig. 8. Representation of the overall spiral stack module (top) and pattern (bottom) for the cost-minimized Archimedean and ideal spiral. In both cases the design in which equal importance is placed on total cost and capital cost is presented. A single membrane is shown in bold and 1/15th of the total cell pairs are included for visual clarity. Membrane width, *W*, is shown for the 1000 L/h case and would scale linearly with production rate.

50% would require a complicated division of flow at the center electrode such that the concentrate stream could be recirculated.

A cross-flow spiral configuration avoids both of these concerns by allowing the diluate stream to flow from inner to outer electrode in a spiral fashion while the concentrate stream flows axially (the direction into the page in Fig. 1). In this configuration, the diluate stream concentration, LCD, and applied current density would still decrease with each successive revolution as desired. Since the electrical resistance and LCD of the diluate stream dominant that of the concentrate, a cross-flow configuration is expected to have minimal affect on the predicted desalination rate and energy consumption numbers presented in Tables 4 and 5. With the two streams hydraulically separated, it would be easier to increase the number of cell pairs and recovery ratio of the system.

5.4. Advantages and limitations of spiral-wound modules

In addition to the potential cost-benefit due to reduced membrane area, a spiral module has a number of other potential benefits:

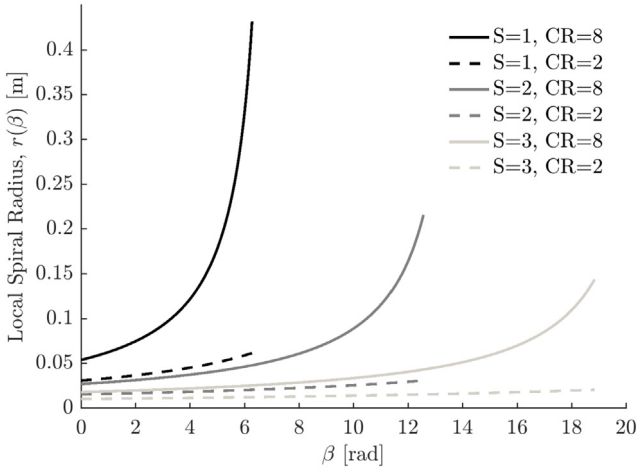

Fig. 10. The local radius of the ideal spiral as a function of angle β for different numbers of total revolutions, S, and concentration ratios, CR.

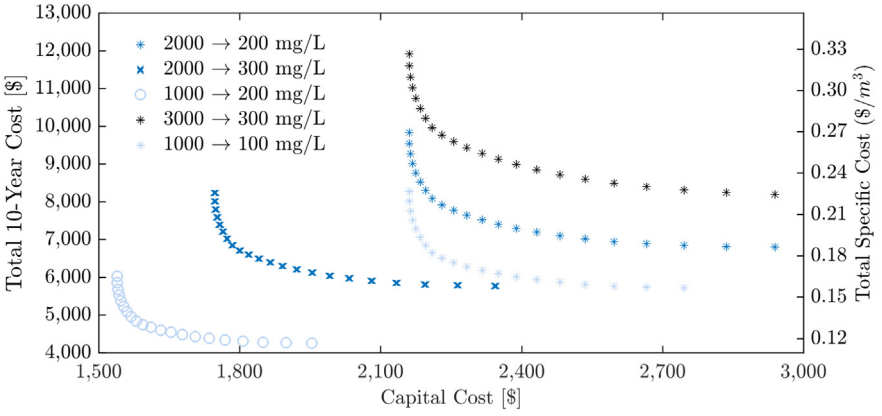

Fig. 9. Capital cost vs. total cost Pareto fronts governing the ideal spiral having different feed and product water concentrations. Note that stacks designed for the same concentration ratio $CR = 10$ represented by the star markers obtain similar capital costs, regardless of the feed water salinity. Significant savings can obtained by increasing the target water salinity.

Table 6
Key ideal spiral stack parameters for the different values of *CR* and *S* shown in Fig. 10. Stack cost and specific energy decrease as the number of revolutions *S* decreases. In all cases $u_{ch} = 6$ cm/s and $h = 0.3$ mm. All tabulated values remain the same regardless of the feed water concentration, except the specific energy for desalination, which is shown for the case of $C^b_{d,0} = 2000$ mg/L.

CR [–]	S [–]	r_0 [cm]	r_S [cm]	W [cm]	N [–]	$A_{electrode}$ [m^2]	$A_{membrane}$ [m^2]	Stack Cost [$]	Γ_{desal} [kWh/m^3]	Γ_{pump} [kWh/m^3]
8	1	5.4	43.2	10	199	0.29	34.98	2102	0.48	0.16
8	2	2.7	21.6	160	12	2.44	32.05	4533	0.53	0.15
8	3	1.8	14.4	480	4	4.88	31.45	7434	0.60	0.14
2	1	3.1	6.2	107	18	0.62	10.39	1264	0.34	0.05
2	2	1.5	3.1	640	3	1.86	10.34	2750	0.42	0.05
2	3	1.0	2.1	1919	1	3.72	10.33	4982	0.54	0.05

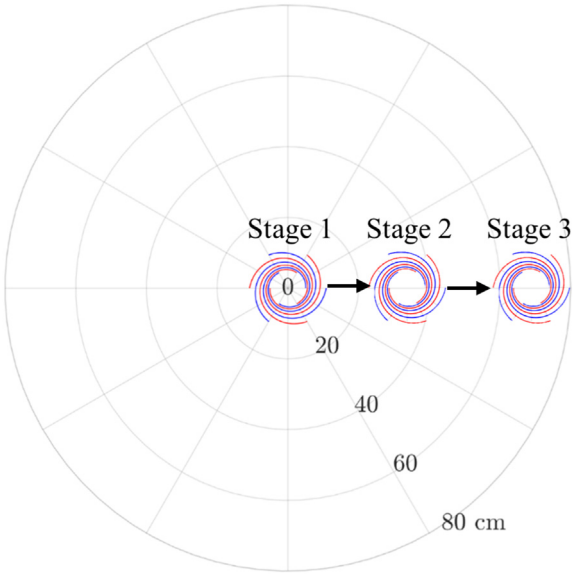

Fig. 11. Representation of the cost-minimized 3-stage ideal spiral pattern, shown on the same grid as the single-stage Archimedean and ideal spiral shape representations from Fig. 8. Note that the inner and outer diameter of each 3-stage spiral is substantially smaller than the single-stage designs capable of achieving the same concentration reduction.

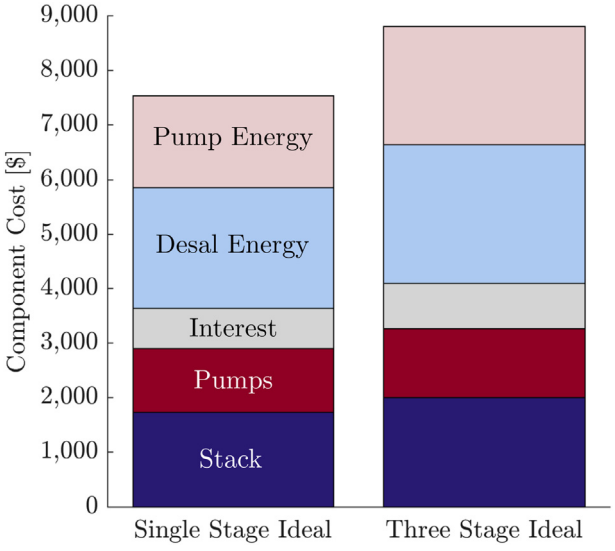

Fig. 12. Breakdown of the total 10-year cost for a system achieving the full concentration reduction in a single ideal spiral stack (*CR* = 10) vs over three ideal spiral stacks in series (*CR* = 2.15 for each).

1. If similar module dimensions to those already installed in reverse osmosis (RO) plants are feasible, it may be possible to utilize existing infrastructure to retrofit a RO plant with ED.
2. Conventional ED stacks are assembled by placing each membrane-spacer pair on top of the previous, either manually or by using a robotic arm. Spiral modules may be able to take advantage of roll-to-roll manufacturing, reducing assembly costs.
3. Conventional ED stacks have a sealed perimeter surrounding the open channel area and entrance ducts that acts as a gasket and prevents flow from leaking out the sides of the stack. This perimeter decreases the active membrane area. A spiral ED stack would likely reduce the size of the required perimeter by removing the sealing at the entrance and exit of the flow paths, thus increasing the proportion of active to total membrane area.

Potential limitations include:

1. Difficulty in replacing individual electrodes or membranes if their lifetime is shorter than that of the entire module.
2. Difficulty in conducting inspection of the ED stacks, including operations such as stack probing, which is common in plants using conventional ED stacks.
3. Difficulty in designing electrode rinse compartments that do not interfere with the diluate stream flow path.

Note that this final point could be critical to the success of spiral ED stacks moving forward. If platinum-coated titanium electrodes are used, as has been the standard for conventional ED systems, a separate electrode rinse stream is implemented. This stream acts to remove from the system the gases (O_2, H_2, and Cl_2) that are created as a result of the oxidation and reduction reactions occurring at the electrodes. Note that the prototype stack tested in this study did not have a separate electrode rinse stream. Determining a way to plumb this external rinse is a critical next step should similar electrodes continue to be used.

It should also be noted, however, that there have been advances in new electrode materials, for example Suez's recently released carbon electrodes for their conventional stacks, which do not produce gas or chemicals and thus eliminate the need for a separate rinse stream [17]. Since carbon electrodes behave in a capacitive nature, they do require operating in electrodialysis reversal (EDR), where the electric polarity on the stack is reversed at set time intervals. We encourage future investigation into the design and manufacturing of cylindrical carbon electrodes, which are expected to be less than half of the cost of the conventional metal electrodes [18], and eliminate the need for the electrode rinse.

6. Conclusions

This work presents an analytical model for a parallel flow, spiral-wound electrodialysis (ED) module. The model builds upon existing work by accounting for channel properties (such as spacer geometry) and LCD. Given a set membrane and spacer type, the shape of the Archimedean spiral that allows for matching applied and limiting current densities at both the inner and outer electrode is a function of the feed and product water concentrations, number of revolutions of the

spiral, number of cell pairs, and linear flow velocity alone. A prototype stack was built and tested experimentally. The experimental results were within 15% of modeled values for all measured parameters.

A cost-minimized design for an Archimedean spiral that has matching applied and adjusted limiting current densities at the inner and outer electrode was determined. Because the effective membrane area increases linearly with each successive revolution, this standard spiral shape is unable to maintain matching limiting and applied current densities along the entire length of the spiral. A novel ideal spiral shape is thus described whose radius grows at the rate required for exact matching at all locations. By analyzing the capital and 10-year total cost Pareto front at the point that places equal weight on the two objectives, we found that the ideal spiral has the potential to reduce the total cost by 21% and capital cost by 39% with respect to an Archimedean spiral. Both designs had large outer electrode radii (49.8 cm and 75.2 cm for the Archimedean and ideal spirals, respectively), thus a discussion on the benefits and drawbacks of staging multiple, smaller radii spiral stacks in series is presented. Cost-minimization for all cases is achieved by maximizing the number of cell pairs and minimizing the number of revolutions of the spiral.

Further work on this topic is ongoing and includes theoretical performance and cost comparisons between all constant voltage stack architectures (constant voltage batch and continuous flat stack architectures) as well as work on the design and feasibility of the Archimedean and ideal spirals. Specific challenges to be addressed in the spiral design include (1) methods of increasing the recovery beyond 50% (currently dictated by the parallel flow configuration investigated here) by transitioning to a cross-flow configuration, (2) methods of operating in electrodialysis reversal (EDR) in order to extend membrane life and provide the option for utilizing carbon electrodes, and (3) methods of manufacturing the spacer that would be required to produce the ideal spiral shape derived in this work (for example, a concentrate spacer that increases in thickness as it is rolled from the inner electrode). While more information on the cost and feasibility of manufacturing spiral-wound ED stacks is required, the analysis presented here suggests the potential for a cost-effective, constant voltage, and continuous system in which membrane area is minimized by matching the limiting and applied current densities at all locations in the stack.

Notation

Roman Symbols

A	membrane area (m^2)
C	molar concentration (mol/m^3)
C^b	bulk concentration (mol/m^3)
C_d	diluate concentration (mol/m^3)
C_c	concentrate concentration (mol/m^3)
CC	capital cost ($)
CR	concentration ratio (–)
d_f	filament diameter (m)
d_h	hydraulic diameter (m)
D_{aq}	diffusion coefficient of aqueous solution (m^2/s)
E_{total}	total applied voltage (V)
E_{el}	electrode potential (V)
E_{mem}	membrane potential (V)
F	Faraday constant (C/mol)
h	channel height (m)
i	current density (A/m^2)
i_{lim}	limiting current density (A/m^2)
I	total current (A)
j	channel location (–)
J	total number of diluate or concentrate channels between the inner and outer electrode (–)
k	mass transfer coefficient (m/s)
l_f	filament pitch (m)
l_a	AEM membrane thickness (m)
l_c	CEM membrane thickness (m)
L	flow path length (m)
N	number of cell pairs (–)
P	pressure (Pa)
Q	flow rate (m^3/s)
r	local radius (m)
r_0	radius of inner electrode (m)
r_S	radius of outer electrode (m)
R_d^b	area resistance, bulk diluate ($\Omega\,m^2$)
R_c^b	area resistance, bulk concentrate ($\Omega\,m^2$)
R^{mem}	average area resistance of AEM and CEM ($\Omega\,m^2$)
R^{BL}	area resistance, boundary layers ($\Omega\,m^2$)
s	revolution number (–)
S	total number of revolutions (–)
t_{cp}	thickness of one cell pair (m)
t^{mem}	apparent transport number of the counterions in the membranes (–)
t_+	transport number, cations in solution (–)
t_-	transport number, anions in solution (–)
TC	10-year total cost ($)
u_{ch}	spacer-filler channel velocity (m/s)
W	flow path width (m)
z	ion charge number (–)

Greek Symbols

β	local spiral angle (rad)
γ	ratio of applied to limiting current (–)
Γ_{total}	total specific energy (J/m^3)
ϵ	void fraction (–)
η_{pump}	pump efficiency (–)
ι	interest rate (–)
μ	viscosity of aqueous solution (Pa-s)
ρ	density of aqueous solution (kg/m^3)
τ	loan term (years)
$\Upsilon_{\text{interest}}$	total cost of interest ($)
Υ_{pump}	capital cost of one pump ($)
Υ_{energy}	total cost of energy ($)
ϕ_A	area porosity (–)
ϕ	current leakage factor (–)

Acknowledgements

This work was sponsored by Tata Projects, Ltd., UNICEF, USAID, the Tata Center for Technology and Design at MIT, and the National Science Foundation Graduate Research Fellowship under grant No. 1122374. Additionally, the authors would like to thank Sahil R. Shah and Dr. Susan E. Amrose, for their contributions to the flat stack model upon which this analysis is based, and Matthew Reeve and James Benn for their guidance and assistance in building prototype spiral stacks over the last few years.

Appendix A. Cost model

This section outlines the cost analysis used to estimate the capital and total 10-year cost of the spiral-wound ED system. Note that the primary goal is to determine the overall trends and trade-offs between spiral stack geometries. Component costs that are expected to be relatively constant between the different geometries are not included. Some examples of such components include: the plant shelter, storage tanks, power connections and wiring, bore well, excavation work, installation charges, reversal valves and piping, sensors and instrumentation, controls, DC rectifier, operator

salary, chemicals, and pre-filters. A production rate of 1000 L/h and 10 h of operation daily is used due to interest in spiral wound stacks specifically for use in rural, decentralized desalination plants [14]. However, the production rate determines the width of the membranes and electrodes only in this analysis; thus stack costs would scale linearly with production rate.

A.1. Capital cost

In this analysis the capital cost includes the cost of the ED stacks' membranes, spacers, and electrodes and the cost of the first set of pumps (brine and diluate). Following the industry-standard operating procedure, we assume equal flow-rates (Q) in the diluate and concentrate channels so that the effects of trans-membrane pressure differences could be neglected. With equal flow rates, channel dimensions, and spacer geometry in the diluate and concentrate fluid circuits, the pressure drop over the stack is also equal and the same size pump could be used for both. Capital cost CC is calculated as

$$CC = 2\Upsilon_{pump} + 2NLW(\Upsilon_{mem} + \Upsilon_{sp}) + 2\pi W(r_0 + r(\beta_f))\Upsilon_{el}, \tag{A.1}$$

where Υ_{pump} is the cost of a single pump ($) and Υ_{mem}, Υ_{sp}, and Υ_{el} are the membrane, spacer, and electrode costs, respectively ($/m^2). The component costs are summarized in Table A.7 and were estimated based on wholesale supplier costs, previous literature, and conversation with an industrial ED stack manufacturer. Note that while this component cost breakdown results in an effective cost of $100/m^2 cell pair, it is distinct from the analysis used in other cost-optimization papers [2,19,20] in which all capital equipment costs are approximated by a lumped cost of $300/m^2 cell pair. This was done intentionally as we needed to capture the cost of the relatively small inner electrode and large outer electrode. Additionally, separating component costs allowed us to capture the capital cost of the pumps.

Table A.7
Unit cost of stack components.

Component	Cost	Reference
Electrodes	$1200/m^2	[18,21,22]
Membranes	$40/m^2	[18,22,23]
Spacers	$10/m^2	[18,22,24]

Data sheets and quotes for Lubi Pumps' LCRN vertical multistage centrifugal 316SS pump line were used to develop a pump cost model. Eq. (A.2) is the result of linear regression of the pump cost Υ_{pump} as a function of pressure P (kPa) and flow rate Q (m^3/h) at the pump's maximum efficiency point. The data for two pump lines (LCRN10 and LCRN1S) are shown in Fig. A.13 along with the example model lines at 1, 4, and 7 m^3/h.

$$\Upsilon_{pump} = 198.10 + 6.06Q + 0.35P \tag{A.2}$$

Similarly, linear regression was used to estimate the peak efficiency of the pump (η_{pump}) as a function of the flow rate Q (m^3/h) using the same pump data base;[1] the result is given as,

$$\eta_{pump} = 2.24Q + 27.63. \tag{A.3}$$

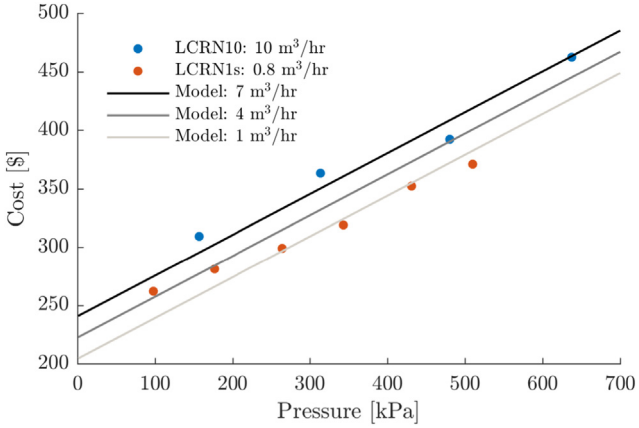

Fig. A.13. Dots are quoted prices for different pumps from Lubi Pumps LCRN1s and LCRN10 pump lines. Specifically, each point represents one of the following pumps: 10-2, 10-4, 10-6, 10-8, 1s-2, 1s-4, 1s-6, 1s-8, 1s-10, and 1s-12. The solid lines are results from the linear regression at three different flow rates. Pump pricing is more heavily dependent on the pressure than the flow rate.

A.2. 10-year total cost

The 10-year total cost of the system TC is calculated as the sum of the CC, interest $\Upsilon_{interest}$, replacements pumps, and energy Υ_{energy} as,

$$TC = CC + \Upsilon_{interest} + 2\Upsilon_{pump} + \Upsilon_{energy}, \tag{A.4}$$

[1] Note that the peak pump efficiency given on the data sheet was scaled by 0.7 before completing the regression to account for the motor efficiency.

where it is assumed one pump replacement is required at year five and the interest is calculated as,

$$\Upsilon_{\text{interest}} = \tau \frac{(CC)\iota(1+\iota)^{\tau}}{(1+\iota)^{\tau}-1} \tag{A.5}$$

where ι is the interest rate and τ is the loan term in years. Based on the typical loan that is available to entrepreneurs for small-scale desalination in rural India, the interest rate is set to 10% and the loan term 5 years [25]. The total cost of energy over 10 years is calculated as

$$\Upsilon_{\text{energy}} = V_{\text{total}} \Gamma_{\text{total}} r_E, \tag{A.6}$$

where V_{total} is the total volume of water produced over the assumed product lifetime of 10 years (m^3), Γ_{total} is the is the total specific energy consumption (desalination plus pumping, kWh/m^3), and r_E is the energy rate, approximated as \$0.10/kWh.

Appendix B. Example calculation

Example calculation steps used to determine the two cost-objectives for the Archimedean spiral in the cost-minimization problem of Section 4 are given here.

1. Calculate the total number of revolutions required to achieve the desired concentration change, given the design variables h, u_{ch}, and N:

$$S = \left[\left(\frac{u_{ch}^{1/2}\xi}{t_{cp}N} \right) \left(\frac{C_{d,0}^2 - C_{d,J}^2}{C_{d,0}C_{d,J}} - 2 \right) \right]^{1/2}$$

2. Calculate the radius of the inner electrode, r_0, such that $i = i_{lim}$ at the beginning of the spiral (Eq. (9)).
3. Calculate the maximum number of cell pairs that can start from the inner electrode (Eq. (14)). If $N < N_{\max}$, continue with calculation.
4. Calculate the length, L, and width, W, of a single membrane (Eqs. (2) and (3)).
5. Calculate the area of membrane segments (Eq. (5)).
6. Calculate the current I that is required to achieve the desired concentration change (Eq. (6)).
7. Calculate the concentration reduction in each revolution (Eq. (7)).
8. Calculate the membrane potential and area resistances at each segment [8] and use to calculate the voltage potential across the stack (Eq. (10)).
9. Calculate the specific energy for desalination and pumping (Eq. (11)).
10. Calculate the capital and 10-year total cost for the system (Appendix A).

References

[1] K.H. Meyer, W. Strauss, La perméabilité des membranes VI. Sur le passage du courant électrique à travers des membranes sélectives, Helv. Chim. Acta 23 (1940) 795–800.
[2] H.-J. Lee, F. Sarfert, H. Strathmann, S.-H. Moon, Designing of an electrodialysis desalination plant, Desalination 142 (2002) 267–286.
[3] S.R. Shah, N.C. Wright, P.A. Nepsky, A.G. Winter, Cost-optimal design of a batch electrodialysis system for domestic desalination of brackish groundwater, Desalination 443 (2018) 198–211.
[4] T. Arden, G. Solt, Improvements in electrolytic apparatus. British Patent GB759275A, 1953.
[5] G.S. Solt, T. Wen, Modeling the spirally wound electrodialysis process: single start, parallel flow, Inst. Chem. Eng. Symp. Ser. 127 (1992) 11–22.
[6] T. Wen, G.S. Solt, Y. Sun, Modeling the cross flow spirally wound electrodialysis SpED process, Desalination 103 (1995) 165–176.
[7] T. Wen, G.S. Solt, Y. Sun, Spirally wound electrodialysis SpED modules, Desalination 101 (1995) 79–91.
[8] N.C. Wright, S.R. Shah, S.E. Amrose, A.G. Winter, A robust model of brackish water electrodialysis desalination with experimental comparison at different size scales, Desalination 443 (2018) 27–43.
[9] D. Nwal Amang, S. Alexandrova, P. Schaetzel, The determination of diffusion coefficients of counter ion in an ion exchange membrane using electrical conductivity measurement, Electrochim. Acta 48 (18) (2003) 2563–2569.
[10] R. Stokes, The diffusion coefficients of eight uni-univalent electrolytes in aqueous solution at 25C, J. Am. Chem. Soc. 72 (5) (1950) 2243–2247.
[11] R. Allgood, A. Gordon, The variation of the transference numbers of sodium chloride in aqueous solution with temperature, J. Chem. Phys. 10 (1942) 124–126.
[12] R.K. McGovern, A.M. Weiner, L. Sun, C.G. Chambers, S.M. Zubair, J.H. Lienhard V, On the cost of electrodialysis for the desalination of high salinity feeds, Appl. Energy 136 (December 2014) 649–661.
[13] F.N. Ponzio, A. Tamburini, A. Cipollina, G. Micale, M. Ciofalo, Experimental and computational investigation of heat transfer in channels filled by woven spacers, Int. J. Heat Mass Transf. 104 (2017) 163–177.
[14] N.C. Wright, A.G. Winter V, Justification for community-scale photovoltaic-powered electrodialysis desalination systems for inland rural villages in India, Desalination 352 (2014) 82–91.
[15] American Water Works Association, Electrodialysis and Electrodialysis Reversal: Manual of Water Supply Practices, (1995).
[16] K.M. Chehayeb, D.M. Farhat, K.G. Nayar, J.H. Lienhard V, Optimal design and operation of electrodialysis for brackish-water desalination and for high-salinity brine concentration, Desalination 420 (2017) 167–182.
[17] Suez Water Technologies & Solutions, Carbon Electrodes for EDR Fact Sheet, (2017).
[18] J. Vinsant, Personal Conversation With Mr. Jamie Vinsant, Suez Water Technologies & Solutions, February 2017.
[19] R.K. McGovern, S.M. Zubair, J.H. Lienhard V, The cost effectiveness of electrodialysis for diverse salinity applications, Desalination 348 (2014) 57–65.
[20] P. Tsiakis, L. Papageorgiou, Optimal design of an electrodialysis brackish water desalination plant, Desalination 173 (2005) 173–186.
[21] Baoji Changli Special Metal Co. Ltd., Shaanxi, China, Platinized Titanium Anode, (2014).
[22] K.G. Nayar, P. Sundararaman, J.D. Schacherl, C.L. O'Connor, M.L. Heath, M.O. Gabriel, S.R. Shah, N.C. Wright, A.G. Winter V, Feasibility study of an electrodialysis system for in-home water desalination in urban India, Dev. Eng. 2 (2016) 38–46.
[23] Hangzhou Iontech Environmental Co. Ltd., Zhejiang, China, IONSEP Membranes, (2014).
[24] Weihai Cortec International Trade Co. Ltd., Shandong, China, Plastic Spacer for RO Membrane Rolling, (2015).
[25] A. Kumar, Personal Conversation with Mr. Anand Kumar, Tata Projects Water Purification Plant Development Center, Secunderabad, India, January 2014.